Dual Cardiac and Respiratory Gated Thoracic Imaging via Adaptive Gantry Velocity and Projection Rate Modulation on a Linear Accelerator: A Proof-of-Concept Simulation Study

Tess Reynolds^{1*}, Chun-Chien Shieh¹, Paul J. Keall¹ and Ricky T. O'Brien¹,

¹ACRF Image X Institute, Faculty of Medicine and Health, The University of Sydney, Sydney, NSW, 2006, Australia.

*corresponding author contact: tess.reynolds@sydney.edu.au

Mailing address: Level 2, Biomedical building (C81), 1 Central Ave, Australian Technology Park, Eveleigh NSW 2015.

Abstract Purpose: Cardiac motion is typically not accounted for during pre-treatment imaging for central lung and mediastinal tumors. However, cardiac induced tumor motion averages 5.8mm for esophageal tumors and organs 3-5mm for some lung tumors, which can result in positioning errors. Our aim is to reduce both cardiac- and respiratory-induced motion artefacts in thoracic cone beam computed tomography (CBCT) images through gantry velocity and projection rate modulation on a standard linear accelerator (linac).

Methods: The acquisition of dual cardiac and respiratory gated CBCT thoracic images were simulated using the XCAT phantom with patient-measured respiratory and ECG traces. The gantry velocity and projection rate were modulated based on the cardiac and respiratory signals to maximize the angular consistency between adjacent projections in the gated cardiac-respiratory bin. The mechanical limitations of a gantry-mounted CBCT system were investigated. For our protocol, images were acquired during the 60-80% window of cardiac phase and 20% displacement either side of peak exhale of the respiratory cycle. The comparator method was the respiratory-only gated CBCT acquisition with constant gantry speed and projection rate in routine use for respiratory correlated (4D) CBCT. All images were reconstructed using the Feldkamp-Davis-Kress (FDK) algorithm. The This article has been accepted for publication and undergone full peer review but has not been through the copyediting, typesetting, pagination and proofreading process, which may lead to differences between this version and the Version of Record. Please cite this article as doi: 10.1002/mp.13670

methods were compared in terms of image sharpness as measured by the edge response width (ERW) and contrast as measured by the contrast-to-noise ratio (CNR). The effects of the total number of projections acquired and magnitude of cardiac motion on scan time and image quality were also investigated.

Results: Median total scan times with our protocol ranged from 117 s (40 projections) through to 296 s (100 projections), compared with 240 s for the conventional protocol (1320 projections). The scan times were dictated by the number of projections acquired, heart rate, length of the respiratory cycle and mechanical constraints of the CBCT system. Our protocol was able to provide between a 8% and 43% decrease in the median value of the ERW in the AP direction across the 17 traces when there was 0.5 cm of cardiac motion and between a 35% and 64% decrease when there was 1.0 cm of cardiac motion over conventional acquisition. In the SI direction, our protocol was able to provide between a 22% and 26% decrease in the median value of the ERW across the 17 traces when there was 0.5 cm of cardiac motion and between a 35% decrease when there was 1.0 cm of cardiac motion over conventional acquisition. In the SI direction, our protocol was able to provide between a 22% and 26% decrease in the median value of the ERW across the 17 traces when there was 0.5 cm of cardiac motion and between a 30% and 35% decrease when there was 1.0 cm of cardiac motion over conventional acquisition. The magnitude of the cardiac motion did not have an observable effect on the median value of the CNR. Across all 17 traces, our adaptive protocol produced noticeable more consistent, albeit lower CNR values compared with conventional acquisition.

Conclusion: For the first time, the potential of adapting CBCT image acquisition to changes in the patient's cardiac and respiratory rates simultaneously for applications in radiotherapy was investigated. This work represents a step towards thoracic imaging that reduces the effects of both cardiac and respiratory motion on image quality.

Keywords: radiotherapy, adaptive, CBCT, imaging, cardiac

Introduction

The development of respiratory correlated cone-beam computed tomography (CBCT) has facilitated advancements in high precision radiotherapy treatments for lung cancer patients, enabling higher radiation doses in fewer fractions to be delivered ¹⁻⁴. However, the treatment of central lung and mediastinal tumors is more difficult due to the proximity to the heart and mediastinum, which are both influenced by cardiac and respiratory motion ⁵⁻⁷. Notably, observable cardiac motion in key organs at risk ⁸⁻¹⁰ are currently not accounted for. The oesophagus, for example, has been observed to have an average of 5.8 mm of motion ¹¹. Additionally, the heart is compressed over the course of a respiratory cycle, leading to volume differences in images acquired at peak exhale and inhale ¹². Uncertainties in tumor and organ motion/volume as a result of cardiac motion are typically accounted for with

increased tumor margins. Additionally, not accounting for tumor motion in the CBCT images acquired immediately prior to treatment can lead to patient positioning errors ^{8,9}.

On linear accelerators (linac) 4D cone beam computed tomography (4DCBCT) systems are now in widespread use for respiratory motion management. In conventional 4DCBCT imaging, patients are imaged with a single constant speed gantry rotation and a constant kV projection pulse rate. The projection acquisition occurs independent of changes in the patient's cardiac and respiratory rates. One way to approach the problem of accounting for both cardiac and respiratory motion is to simply gate in both cardiac phase and respiratory displacement, reconstructing when motion is minimized in the overlapping physiological bins. However, due to the constant gantry speed and kV projection rate, projection clustering and under sampling of the angular scan range occur within the dual gated bins. This results in low quality reconstructed images due to the appearance of streak artefacts. These problems are well known for respiratory correlated imaging (4D) CBCT but are magnified for dual cardiac and respiratory imaging.

Previously, we have developed and tested methods to regulate the velocity of the gantry and projection time interval in response to the patient's real-time respiratory signal ¹³⁻¹⁵. Importantly, these methods have already been implemented on an Elekta Synergy linear accelerator (linac) for respiratory motion guided imaging, displaying significant improvements in the image quality for the same dose as well as enabling up to a 70% reduction in imaging dose for the same original image quality ¹⁶. Extending this concept to conduct cardiac motion guided imaging we have developed a gated CBCT imaging protocol, which regulates the gantry velocity and projection time interval in accordance with the patient's real-time electrocardiogram (ECG), under breath hold conditions ¹⁷. Here, we look to combine these techniques to allow dual cardiac and respiratory gated thoracic CBCT imaging without breath hold, Figure 1.

I. Materials and Methods

The main aim of conducting dual cardiac and respiratory gated image acquisition with our adaptive protocol is to minimize the effects of both cardiac and respiratory motion on image quality. To achieve higher image quality over conventional constant gantry velocity and projection rate acquisition protocols, our adaptive protocol looks to reduce the variation in angular separation between adjacent projections by utilizing two additional degrees of freedom during the acquisition process. Namely, adapting the gantry velocity and projection rate in accordance to both the patient's ECG and respiratory traces. To understand and characterize the performance of utilizing our adaptive protocol for dual cardiac and respiratory imaging for applications in radiotherapy, a series of simulated scans were performed.

A. Adaptive Dual Cardiac and Respiratory Acquisition Protocol

We use both the patient's ECG and respiratory trace to adaptively determine the gantry velocity and projection rate of a conventional linac with on board kV imager during a single sweep acquisition. The precise movements that the gantry undertakes during a scan is determined by the desired number of projections to be acquired, the mechanical constraints of the imaging system and the patient's physiological signals (i.e. cardiac and respiratory rates), where previous physiological rates are used to assist in predicting future rates. A flowchart of our adaptive algorithm used to acquire the dual cardiac and respiratory gated thoracic images is provided in Figure 2. Here, only a single cardiac acquisition window (one cardiac phase) per cardiac cycle and respiratory acquisition window (one displacement bin) per respiratory cycle are examined. Acquisition only occurs if the requirements of the cardiac acquisition window overlaps with the requirements of the respiratory acquisition window, Figure 1. The details of the algorithms that will be used to determine the cardiac and respiratory acquisition windows for future experimental implementation, including how they are able to cope with variations and irregularities in the patient's physiological signals can be found in our previous studies^{13, 14, 17}.

Due to the weight and bulk of a conventional linac system, the maximum gantry rotation velocity is strictly limited and specified by the IEC standard 60601-2-1 of a maximum gantry velocity of 7 °/s. Therefore, for the simulation scans completed it is assumed that the gantry is capable of rotating at a maximum acceleration of 9 °/s² and velocity of 6 °/s o remain within the maximum gantry rotation velocity limit, and acquires projections at a fixed framerate of 5.5 Hz. This is representative of clinical acquisition protocols commonly used on Elekta linear accelerators and aligns with our previous work on modulating the gantry velocity and projection time interval on an Elekta Synergy linear accelerator¹⁶. These limits on the gantry velocity and framerate restrict the complexity of the variations in the gantry trajectory over the course of the scan.

The precision location of the acquisition window for each physiological window is dictated by the desired application, however, most commonly the location will be where the respective motion is minimized. Here we identify the cardiac acquisition window as being 60-80% through the cardiac cycle, encapsulating the optimal windows for low and intermediate heart rates ¹⁸⁻²⁰, and the respiratory acquisition window as 20% displacement either side of peak exhale of the most recent cycle, as this is where the respiratory motion is most stable for a longest period of time.

The influence of total number of projections acquired on total scan time and image quality using our adaptive protocol is also considered. Adaptive acquisitions with 40, 75 and 100 projections, representing an average angular separation of 5° , 2.67° and 2° respectively were considered. The angular scan range for both our adaptive and the conventional protocol was 200°.

To maintain an even angular separation between projections our adaptive protocol will only acquire a single projection per dual cardiac and repository acquisition window. This has been shown to maintain image quality while eliminating duplicate projections for respiratory triggered 4DCBCT²¹. Instead of rotating with constant velocity, the gantry undertakes a series of forward acceleration and deceleration movements in accordance to changes in the patient's cardiac and respiratory rates to acquire all required projections, Figure 1 (B). More specifically, the gantry undergoes the following movements during the scan. Initially the gantry is at rest. The patient's cardiac and respiratory signals are monitored, and the current cardiac phase and respiratory displacement are calculated. If the conditions of the dual acquisition window are satisfied, i.e. the respiratory signal is within 20% displacement either side of peak exhale of the most recent cycle and the cardiac phase is between 60-80% of the cardiac cycle, an acquisition occurs. The gantry then repositions itself to the next angular location, using a series of forward acceleration and deceleration movements, ready for the subsequent dual acquisition window. This is repeated until all the required projections have been acquired.

B. Conventional Acquisitions

In current conventional full-fan acquisitions on a conventional linac with an on-board kV imager, the gantry velocity consists of a single forward sweep at constant speed and projection rate, independent of the patient's cardiac and respiratory rates. A standard 4DCBCT scan accounting only for respiratory motion typically consists of 1320 projections acquired over 4 minutes. At the end of the scan the projections are retrospectively sorted into the desired respiratory displacement or phase bins and reconstructed to provide 3D visualization of the patient's anatomy in each bin. As with our adaptive protocol, we select the respiratory acquisition window as 20% displacement either side of peak exhale of the most recent cycle. Again, this is where the respiratory motion is most stable for longer periods of time and enables a direct comparison with our adaptive protocol. However, poor image quality often results due to projection clustering and under sampling within each phase bin due to the constant velocity and projection time interval acquisition.¹⁶.

C. Cardiac and Respiratory Traces

Cardiac and respiratory traces from the Combined measurement of ECG, Breathing and Seismocardiagram (CEBS Database)^{22, 23} were used to compare our adaptive protocol dual gated protocol with the conventional acquisition protocol. The database contains conventional ECG signals, respiratory signals obtained from a thoracic piezoresistive band and seismocardiograms from 20 healthy volunteers lying in supine position, awake, on a single bed. The signals from the volunteers were recorded in three time blocks: 5 minutes with no music, 50 minutes listening to classical music and another 5 minutes with no music. The reason behind utilizing music during the signal acquisition is not specified in the description of the formation of the database. To remove the possibility of signal interruption due to the change from no-music to music, we select the first 8 minutes of the 50 minute

music session as our data set (records m001-m020 in the online database). From this set of 20 traces, 3 pairs of ECG and respiratory signals (m006, m018, m020) were discarded due to noticeable acquisition abnormalities in the respiratory signal. Namely, there is visible interference in the respiratory signal from the ECG signal resulting in a noisy replication of the ECG signal instead of capturing the respiratory motion. Volunteer number 4 is also noted as displaying some ectopy (irregular heart rhythm) in record m004. A summary of the average heart rates and respiratory cycle lengths for the first eight minutes of each trace used in the simulated scans are provide in Table 1.

As the respiratory signals within this database were obtained from a thoracic piezoresistive band, the millivolt recording was converted to displacement for the simulation scans to take place. It was assumed that there was a direct correlation between the millivolt recording and respiratory motion in centimetres, namely, the maximum difference in peak inhale to peak exhale of the trace in millivolts was equal to 1 cm of displacement motion in the SI direction. This conversion was applied to all respiratory traces prior to them being used for the simulated scans.

D. Digital Phantom

The XCAT software phantom is a programmable digital software phantom that simulates realistic moving patient physiology and anatomy ²⁴. Time series of XCAT volumes were generated using the ECG and respiratory traces specified in Table 1, and designated scan parameters discussed above to reconstruct the dual cardiac and respiratory-gated thoracic images. Specifically, the ECG and respiratory traces were directly used for the motion-related parameters within the XCAT parameter initialization file for the surrounding anatomy (i.e. diaphragm, chest-well and heart).

Additionally, a spherical tumor 20 mm in diameter was placed near the heart within the XCAT volume. The position of the tumor was selected to minimize overlap with existing thoracic structures to enable clear visual identification of the tumor, ensuring accurate calculation of the image quality metrics as defined in Figure 3. The spherical tumor was programmed to have motion in both the AP and SI directions to replicate the respective effects of cardiac and respiratory motion on a central lung tumor. For simplification, the motion of the spherical tumor in the AP direction is derived from the ECG trace, while the motion of the spherical tumor in the SI direction is derived from the respiratory trace. That is, the frequency of induced cardiac motion on the spherical tumor in the AP direction was dependent on heart rate and derived from the XCAT's heart motion model. The maximum amount of heart motion over the course of the cardiac cycle was scaled to 0.5 and 1 cm. This encapsulates the range of AP motion central lung tumors ⁹ and organs at risk such as the esophagus ¹¹ have been observed to experience. The induced respiratory motion of the spherical tumor in the SI direction is directly derived from the respiratory traces as described in subsection (C) above.

II.

The XCAT volumes were forward-projected according to the scanning geometry using the Reconstruction Toolkit ²⁵ with Poisson noise modelling 30,000 initial photons per detector element added to generate simulated projections. The 3D images were reconstructed using the Feldkamp-Davis-Kress algorithm ²⁶, again implemented in the Reconstruction Toolkit ²⁵. A tube voltage of 125 kV and 1.0 mm² pixels were used for all image acquisitions. The reconstructed image size was 256×256 pixels. The source to isocenter distance (SID) and the source to detector distance (SDD) were 100.0 cm and 150.0 cm.

E. Image Quality Analysis

The analysis of the reconstructed images was performed by examining the image quality metrics of edge response width (ERW) and contrast to noise (CNR)¹⁴. The ERW provides an indication of the sharpness of the boundary between adjacent regions (i.e. tumor and lung), while the CNR enables an insight into the visibility of anatomical detail within the image. For the calculation of the ERW, linear profiles across the spherical tumor/lung boundary in the AP and SI directions were used, Figure 3 (A). This encapsulated the largest range of motion blur experienced by the spherical tumor due to both the cardiac (AP) and respiratory (SI) motion. From these profile, the ERW is defined as the width between 25% and 75% change in intensity across the linear profile ¹⁴, Figure 3 (B). A lower ERW suggests clearer, more defined boundaries, indicating sharper images. Comparatively, a higher CNR suggests better detail visibility. The CNR is described in equation 1, where I_{object} and $I_{backgound}$ are the intensities of the object and background respectively, as displayed in Figure 3 (A).

$$CNR = \frac{mean(I_{object}) - mean(I_{background})}{\sqrt{\sigma_{I_{object}}^2 - \sigma_{I_{background}}^2}}$$
(1)

II. Results

A. Visual Images

The reconstructed dual cardiac and respiratory gated thoracic images (axial and coronal view) using our adaptive and conventional acquisition protocol for 0.5 and 1.0 cm of induced cardiac motion for the breathing trace and ECG signal from trace ID m001 are shown in Figure 4. All traces follow the same visual trends as displayed by trace ID m0001, with the observable visual variations in the positioning of the tumor arising from fluctuations in the individual breathing traces. Variations in average heart rate had no observable visual effect on the reconstructed images. The axial slice visualized in Figure 4 (A) dissects the spherical tumor, highlighting the maximum observed cardiac induced motion blur in the AP direction. Note that due to the positioning of the tumor within the thorax, this slice does not encapsulate the maximum motion experienced by the heart itself, thus showing minimal motion artifacts across the heart/lung boundary for both acquisition methods. To

highlight motion artefacts on the heart itself, Figure 4 (B) shows the coronal view of the reconstructed images. Noticeable motion blur on the left side of the heart can be observed from the conventional scan, which was significantly reduced in all implementations of our adaptive protocol. Note that the spherical tumor is not visible in the slice visualized in Figure 4 (B).

Overall, the positive effects of respiratory gating on image quality in both acquisition protocols can be observed via the minimal presence of motion artifacts of the surrounding thoracic structures. Further, there is a reduction in the presence of streak artefacts between our adaptive protocol and the conventional protocol, despite the noticeable reduction in projections used to reconstruct the images. Notably, there is a clearly observable reduction in the motion blur in the spherical tumor, Figure 4 inserts.

Table 2 contains the corresponding scan times for the various implementations of our adaptive protocol. The total scan times of our adaptive protocol are heavily dependent on the number of projections being acquired, heart rate and respiratory rates. For example, respiratory trace ID m009 displays periods of elongated breath lengths from 200 to 300 seconds. This negatively impacts the total scan time for our adaptive protocol compared with the conventional protocol as long periods of time are spent waiting for the conditions of the dual acquisition window. However, the elongated breath lengths will also negatively impact the conventional protocol through the reconstructed image quality. This is because there is little change in gantry angle within the respiratory displacement acquisition window, so each acquired projection provides almost the identical anatomical information.

It is also important to note that in the conventional scans, an average of 358 projections are retrospectively selected out of the 1320 acquired to reconstruct the images from 20% displacement either side of peak exhale.

B. Edge Response Width

Boxplots of the ERW in the AP and SI direction for all traces and ranges of cardiac motion for both our adaptive and the conventional protocol are provided in Figure 5. Note, there is no motion of the phantom in the LR direction, only in SI and AP. With a maximum of 0.5 cm of cardiac motion, our adaptive protocol results in a decrease in median ERW in the AP direction compared to the conventional acquisition from 2.6 mm down to 2.4 mm (40 projections), 1.7 mm (75 projections) and 1.5 mm (100 projections) respectively. That is, up to a 43% improvement in the image sharpness can be achieved in the AP direction. This confirms the visual increase in image sharpness with respect to the spherical tumor apparent in Figure 4. In the case of 1.0 cm of cardiac motion, our adaptive protocol results in a decrease in median ERW in the AP direction compared to the conventional acquisition from 4.8 mm to 3.1 mm (40 projections), 1.8 mm (75 projections) and 1.6 mm (100

projections) respectively. Again, this corresponds to an improvement in image sharpness of up to 64% in the AP direction. Overall, our adaptive protocol is observed to provide a more consistent ERW in the AP direction across all traces considered.

In the SI direction and with 0.5 cm of cardiac motion, our adaptive protocol results in a decrease in the median ERW compared to the conventional acquisition from 2.5 mm down to 1.8 mm (40 projections), 1.9 mm (75 projections) and 1.8 mm (100 projections) respectively. That is, up to a 26% improvement in the image sharpness can be achieved in the SI direction for 0.5 cm of cardiac motion. In the case of 1.0 cm of cardiac motion, our adaptive protocol results in a decrease in median ERW in the SI direction compared to the conventional acquisition from 2.8 to 1.9 mm (40 projections), 1.9 mm (75 projections) and 1.8 mm (100 projections) respectively. This corresponds to an improvement in image sharpness of up to 35% in the SI direction for 1.0 cm of cardiac motion. Again, our adaptive protocol is observed to provide a more consistent ERW in the SI direction across all traces considered.

Contrast to Noise Ratio

Boxplots of the CNR for all traces, protocols (adaptive and conventional) and levels of cardiac motion are provided in Figure 6. The results indicate that our adaptive protocol can provide a tradeoff between image contrast and total scan time. Our adaptive protocol provides tighter spread of the 25th and 75th percentiles across all 17 traces and numbers of projections acquired compared with the conventional acquisition. This indicates more consistent CNR even with variations in the individual patient ECG and breathing traces. The median value of the CNR with the conventional acquisition is 21.2 for 0.5 cm of cardiac motion and 20.2 for 1.0 cm of cardiac motion. The median conventional acquisition CNR is higher than all three implementations of our adaptive protocol for 0.5 cm of cardiac motion; 8.8 for 40 projections, 17.1 for 75 projections and 21.0 for 100 projections. For 1.0 cm of cardiac motion, the median CNR of our adaptive protocol acquiring 100 projections is slightly higher (20.7) than the conventional acquisition. Further, using our adaptive protocol and acquiring 40 projections results in a median CNR of 8.9 and acquiring 75 projections results in a median CNR of 16.9. This indicates overall that the magnitude of the cardiac motion (0.5 cm or 1.0 cm) does not have an observable effect on the median value of the CNR for either our adaptive or the conventional protocol. The increased CNR of the conventional protocol is the result of more projections being used to reconstruct the images. An average of 358 projections are used in the conventional acquisition compared to only 40, 75 and 100 for our adaptive protocol.

III. Discussion

Our results show that for the first time, dual cardiac and respiratory gated thoracic imaging is feasible on a conventional linac with on board kV imager under free breathing conditions. Specifically, our adaptive protocol has the potential to successfully modulate the gantry velocity and projection rate with respect to both a patient's evolving cardiac and respiratory rates. Additionally, by comparing to current conventional acquisition protocols, noticeable improvements in image quality can be observed through the control of the angular separation between projections. Finally, although the main aim was to improve image quality, our adaptive protocol has shown the potential to reduce overall imaging dose by utilizing fewer projections for image reconstruction.

The improved performance of our adaptive protocol over the conventional protocol was most noticeable in the image sharpness, through the ERW in the AP direction, of the spherical tumor placed near the heart. This is not completely unexpected as for this simulation study this is the direction of cardiac motion and the conventional protocol currently has no way of accounting for cardiac motion. Our adaptive protocol also provided improvement in the image sharpness through the ERW in the SI direction over the conventional protocol. However, this was not as pronounced as the conventional protocol is able to retrospectively isolate respiratory bins to perform the image reconstruction.

Importantly, our adaptive protocol provides increased flexibility over the current conventional protocols by enabling a trade-off between image quality and total scan time. For example, our adaptive protocol enables a low projection count scan that still results in improved image sharpness, even if the image contrast is reduced. Notably, the mean scan time for this low projection scan is almost 2 minutes faster than the conventional scan. However, for no additional mean scan time compared to the conventional protocol, clear improvements in both the image sharpness and contrast can be observed visually and through the image quality metrics. The development of the next generation of imaging and treatment devices could assist in reducing scan times further as higher gantry accelerations and velocities can be realized.

The current implementation of our adaptive protocol utilizes the standard FDK algorithm for image reconstruction, however, there is potential to combine with alternative reconstruction methods to provide additional improvements in image quality. For example, more advanced reconstruction methods such as Prior Image Constrained Compressed Sensing (PICCS)²⁷ and McKinnon Bates (MKB)²⁸ have shown potential in suppressing streaking artefacts in 4D CBCT images. Further, specific iterative reconstruction methods relying on motion vector fields to reconstruct the images for dual binned scans, thereby realizing 5DCBCT, have already been developed ²⁹. However, computation times are currently long with all iterative reconstruction methods. This hinders these approaches finding widespread use in radiotherapy.

There are currently a limited number of readily available database resources containing simultaneously measured patient ECG and breathing traces. This simulation study used combined cardiac and respiratory traces in the CEBS database, which were collected from healthy volunteers. As such, both the ECG and respiratory traces are not expected to show the same level of potential

variation and irregularities associated with lung cancer patients. However, in our previous work developing and testing cardiac- and respiratory- only motion guided CBCT imaging protocols separately we investigated and characterised the performance of each protocol's ability to handle variations and irregularities in the patient's physiological signal being considered. That is, for cardiac-only motion guided CBCT imaging we considered the effect of arrhythmias on image quality and scan time¹⁷, while for respiratory-only motion guided CBCT imaging we looked to encompass irregular breathing by examining 112 breathing traces from 24 lung cancer patients¹⁴.

We have previously demonstrated the feasibility of modifying the gantry velocity and projection time interval in response to a patient's real-time respiratory signal on an Elekta linac ^{15, 16}, indicating the potential to move our dual adaptive protocol from simulation through to experimental realization. The movements of the gantry are smooth, not requiring rapid repositioning, and are within the mechanical constraints of a standard linac. However, key challenges may arise in running the protocol in practice. Notably, this will include integrating synchronized cardiac and respiratory monitors with the linear accelerator electronics. Additionally, the effects of potential latencies need to be investigated for each system and taken into account.

There have been ongoing efforts in reducing motion artefacts to improve CBCT image quality. The benefits of going from 3D imaging (no motion correlation) to 4D imaging (respiratory motion correlation) have been well documented in the literature ^{1, 30, 31}. This work represents a step towards full 5D thoracic imaging with single phase, dual cardiac and respiratory (4D) CBCT acquisition that reduces the effect of both cardiac and respiratory motion on image quality. The clinical applications of the current cardiac and respiratory gated CBCT protocol includes cases in gated radiotherapy, such as, treating central lung lesions with SABR where cardiac damage and toxicities are a concern^{32, 33}. To overcome the limitations of increased scan time with the low duty cycle, the treatment could be delivered with high output linacs or even FLASH radiotherapy³⁴. FLASH radiotherapy, where the dose is delivered in extremely short time intervals, may require cardiac and respiratory gated CBCT to avoid delivering large amounts of dose to the wrong place. Additionally, to incorporate our adaptive protocol into current treatment workflows, the planning CT would need to be completed in breath-hold at an inhalation level that matches the planned free breathing phase used for treatment.

The next step is to extend this protocol to encompass multiple phases per physiological signal, requiring a more advanced mathematical optimization of the ideal gantry trajectory. A minimum extension of our adaptive protocol for future applications would include four phases, namely, two cardiac (diastole and systole) and two respiratory (peak inhale and peak exhale). Due to the speed of transition through some respiratory phases, there may be incomplete data in some respiratory/cardiac phase bins challenging conventional FDK reconstruction. Thus, coupling the image acquisition with

projection sharing techniques³⁵ and motion compensated reconstruction techniques²⁹ may be necessary.

IV. Conclusions

For the first time, we have described and presented simulation results of our adaptive protocol for dual cardiac and respiratory gated thoracic imaging via the adaptive regulation of the gantry velocity and projection time interval using the patient's cardiac and respiratory signals on a linear accelerator. This work represents a step towards complete cardiac and respiratory motion management during radiotherapy treatments.

Acknowledgements

Ricky O'Brien would like to acknowledge the support of a Cancer Institute of NSW Career Development Fellowship. Paul J. Keall acknowledges the support of an Australian NHMRC Senior Principal Research Fellowship. Chun-Chien Shieh acknowledge the support from the Australian Government National Health and Medical Research Council Early Career Fellowship APP1120333, and Cancer Institute New South Wales Early Career Fellowship CS00481. This grant #1123068 was awarded through the Priority-driven Collaborative Cancer Research Scheme and funded by Cancer Australia. The authors would also like to acknowledge ACRF Image X Institute Design and Communication Officer Julia Johnson for graphical support.

V. References

- . J.J. Sonke, L. Zijp, P. Remeijer, and M.v. Herk, "Respiratory correlated cone beam CT". *Medical Physics*. 32(4): p. 1176-1186, 2005.
- S.S. Vedam, P.J. Keall, V.R. Kini, H. Mostafavi, H.P. Shukla, and R. Mohan, "Acquiring a fourdimensional computed tomography dataset using an external respiratory signal". *Physics in Medicine & Biology*. 48(1): p. 45, 2003.
- 3. M. Hiraoka, Y. Matsuo, and Y. Nagata, "Stereotactic body radiation therapy (SBRT) for earlystage lung cancer". *Cancer/Radiothérapie*. 11(1): p. 32-35, 2007.
- 4. M. Koshy, R. Malik, R.R. Weichselbaum, and D.J. Sher, "Increasing Radiation Therapy Dose Is Associated With Improved Survival in Patients Undergoing Stereotactic Body Radiation Therapy for Stage I Non–Small-Cell Lung Cancer". International Journal of Radiation Oncology*Biology*Physics. 91(2): p. 344-350, 2015.
- S. Senthi, M. Dahele, B.J. Slotman, and S. Senan, "Investigating strategies to reduce toxicity in stereotactic ablative radiotherapy for central lung tumors". *Acta Oncologica*. 53(3): p. 330-335, 2014.
- S. Senthi, C.J.A. Haasbeek, B.J. Slotman, and S. Senan, "Outcomes of stereotactic ablative radiotherapy for central lung tumours: A systematic review". *Radiotherapy and Oncology*. 106(3): p. 276-282, 2013.
- 7. R. Timmerman, R. McGarry, C. Yiannoutsos, L. Papiez, K. Tudor, J. DeLuca, M. Ewing, R. Abdulrahman, C. DesRosiers, M. Williams, et al., "Excessive Toxicity When Treating Central

Tumors in a Phase II Study of Stereotactic Body Radiation Therapy for Medically Inoperable Early-Stage Lung Cancer". *Journal of Clinical Oncology*. 24(30): p. 4833-4839, 2006.

- 8. T. Chen, S. Qin, X. Xu, S.K. Jabbour, B.G. Haffty, and N.J. Yue, "Frequency filtering based analysis on the cardiac induced lung tumor motion and its impact on the radiotherapy management". *Radiotherapy and Oncology*. 112(3): p. 365-370, 2014.
 - Y. Seppenwoolde, H. Shirato, K. Kitamura, S. Shimizu, M. van Herk, J.V. Lebesque, and K. Miyasaka, "Precise and real-time measurement of 3D tumor motion in lung due to breathing and heartbeat, measured during radiotherapy". *International Journal of Radiation Oncology*Biology*Physics*. 53(4): p. 822-834, 2002.
- 10. M.B.M. Hofman, S.A. Wickline, and C.H. Lorenz, "Quantification of in-plane motion of the coronary arteries during the cardiac cycle: Implications for acquisition window duration for MR flow quantification". *Journal of Magnetic Resonance Imaging*. 8(3): p. 568-576, 1998.
- 11. J. Palmer, J. Yang, T. Pan, and L.E. Court, "Motion of the esophagus due to cardiac motion". *PloS one*. 9(2): p. e89126-e89126, 2014.
- 12. E. Weiss, K. Wijesooriya, S.V. Dill, and P.J. Keall, "Tumor and normal tissue motion in the thorax during respiration: Analysis of volumetric and positional variations using 4D CT". *International Journal of Radiation Oncology*Biology*Physics*. 67(1): p. 296-307, 2007.
- 13. R.T. O'Brien, B.J. Cooper, and P.J. Keall, "Optimizing 4D cone beam computed tomography acquisition by varying the gantry velocity and projection time interval". *Physics in Medicine* & *Biology*. 58(6): p. 1705, 2013.
- 14. R.T. O'Brien, B.J. Cooper, J. Kipritidis, C.C. Shieh, and P.J. Keall, "Respiratory motion guided four dimensional cone beam computed tomography: encompassing irregular breathing". *Phys Med Biol.* 59(3): p. 579-95, 2014.
- 15. R.T. O'Brien, U. Stankovic, J.J. Sonke, and P.J. Keall, "Reducing 4DCBCT imaging time and dose: the first implementation of variable gantry speed 4DCBCT on a linear accelerator". *Phys Med Biol.* 62(11): p. 4300-4317, 2017.
- 16. R.T. O'Brien, B.J. Cooper, C.-C. Shieh, U. Stankovic, P.J. Keall, and J.-J. Sonke, "The first implementation of respiratory triggered 4DCBCT on a linear accelerator". *Physics in Medicine* & *Biology*. 61(9): p. 3488, 2016.
- 17. T. Reynolds, C.-C. Shieh, P.J. Keall, and R.T. O'Brien, "Towards patient connected imaging with ACROBEAT: Adaptive CaRdiac cOne BEAm computed Tomography". *Physics in Medicine & Biology*. 64(6): p. 065006, 2019.
- 18. S. Mao, M.J. Budoff, L. Bin, and S.C. Liu, "Optimal ECG trigger point in electron-beam CT studies: three methods for minimizing motion artifacts". *Academic radiology*. 8(11): p. 1107-1115, 2001.
- H. Isma'eel, Y.S. Hamirani, R. Mehrinfar, S. Mao, N. Ahmadi, V. Larijani, S. Nair, and M.J. Budoff, "Optimal phase for coronary interpretations and correlation of ejection fraction using late-diastole and end-diastole imaging in cardiac computed tomography angiography: implications for prospective triggering". *The International Journal of Cardiovascular Imaging*. 25(7): p. 739-749, 2009.
- A.C. Weustink, N.R. Mollet, F. Pugliese, W.B. Meijboom, K. Nieman, M.H. Heijenbrok-Kal, T.G. Flohr, L.A.E. Neefjes, F. Cademartiri, P.J.d. Feyter, et al., "Optimal Electrocardiographic Pulsing Windows and Heart Rate: Effect on Image Quality and Radiation Exposure at Dual-Source Coronary CT Angiography". *Radiology*. 248(3): p. 792-798, 2008.
- 21. J.C. Benjamin, T.O.B. Ricky, K. John, S. Chun-Chien, and J.K. Paul, "Quantifying the image quality and dose reduction of respiratory triggered 4D cone-beam computed tomography with patient-measured breathing". *Physics in Medicine & Biology*. 60(24): p. 9493, 2015.
- 22. M.A. García-González, A. Argelagós, M. Fernández-Chimeno, and J. Ramos-Castro. *Differences in QRS Locations due to ECG Lead: Relationship with Breathing*. 2014. Cham: Springer International Publishing.

- 23. M.A. García-González, A. Argelagós-Palau, M. Fernández-Chimeno, and J. Ramos-Castro. *A* comparison of heartbeat detectors for the seismocardiogram. in Computing in Cardiology 2013. 2013.
- 24. P.W. Segars, G. Sturgeon, S. Mendonca, J. Grimes, and B.M.W. Tsui, "4D XCAT phantom for multimodality imaging research". *Medical Physics*. 37(9): p. 4902-4915, 2010.
- 25. S. Rit, M.V. Oliva, S. Brousmiche, R. Labarbe, D. Sarrut, and G.C. Sharp, "The Reconstruction Toolkit (RTK), an open-source cone-beam CT reconstruction toolkit based on the Insight Toolkit (ITK)". *Journal of Physics: Conference Series*. 489(1): p. 012079, 2014.
- 26. L.A. Feldkamp, L.C. Davis, and J.W. Kress, "Practical cone-beam algorithm". *Journal of the Optical Society of America A*. 1(6): p. 612-619, 1984.
- 27. G.-H. Chen, J. Tang, and S. Leng, "Prior image constrained compressed sensing (PICCS): A method to accurately reconstruct dynamic CT images from highly undersampled projection data sets". *Medical Physics*. 35(2): p. 660-663, 2008.
- 28. G.C. McKinnon and R.H.T. Bates, "Towards Imaging the Beating Heart Usefully with a Conventional CT Scanner". *IEEE Transactions on Biomedical Engineering*. BME-28(2): p. 123-127, 1981.
- 29. S. Sauppe, A. Hahn, M. Brehm, P. Paysan, D. Seghers, and M. Kachelrieß. *Five-dimensional motion compensation for respiratory and cardiac motion with cone-beam CT of the thorax region*. in *SPIE Medical Imaging*. 2016. SPIE.
- 30. R.A. Sweeney, B. Seubert, S. Stark, V. Homann, G. Müller, M. Flentje, and M. Guckenberger, "Accuracy and inter-observer variability of 3D versus 4D cone-beam CT based imageguidance in SBRT for lung tumors". *Radiation Oncology*. 7(1): p. 81, 2012.
- 31. S. Thengumpallil, K. Smith, P. Monnin, J. Bourhis, F. Bochud, and R. Moeckli, "Difference in performance between 3D and 4D CBCT for lung imaging: a dose and image quality analysis". *Journal of applied clinical medical physics*. 17(6): p. 97-106, 2016.
- S.C. Darby, M. Ewertz, P. McGale, A.M. Bennet, U. Blom-Goldman, D. Brønnum, C. Correa, D. Cutter, G. Gagliardi, B. Gigante, et al., "Risk of Ischemic Heart Disease in Women after Radiotherapy for Breast Cancer". New England Journal of Medicine. 368(11): p. 987-998, 2013.
- 33. S.W. Yusuf, S. Sami, and I.N. Daher, "Radiation-induced heart disease: a clinical update". *Cardiology research and practice*. 2011: p. 317659-317659, 2011.
- 34. V. Favaudon, L. Caplier, V. Monceau, F. Pouzoulet, M. Sayarath, C. Fouillade, M.-F. Poupon, I. Brito, P. Hupé, J. Bourhis, et al., "Ultrahigh dose-rate FLASH irradiation increases the differential response between normal and tumor tissue in mice". *Science Translational Medicine*. 6(245): p. 245ra93-245ra93, 2014.
- 35. R.T. O'Brien, J. Kipritidis, C.-C. Shieh, and P.J. Keall, "Optimizing 4DCBCT projection allocation to respiratory bins". *Physics in Medicine and Biology*. 59(19): p. 5631-5649, 2014.

Figure 1. Dual cardiac and respiratory gated thoracic Cone Beam Computed Tomography imaging using our adaptive protocol, which determines the gantry velocity and projection time interval in accordance with the patient's ECG and respiratory signals.

Figure 2. A flowchart showing the main algorithm controlling our adaptive protocol during dual cardiac and respiratory imaging.

Figure 3. (A) Axial view showing the linear profile in the AP direction (red) and homogenous regions I_{object} and $I_{background}$ (green) used for the ERW in the AP direction and CNR calculations respectively. (B) Coronal view showing the linear profile in the SI direction (orange) used for the ERW in the SI direction calculation. (C) Example of the linear intensity profiles from trace ID m001 for our adaptive (blue) and conventional (black) acquisitions showing the definition of ERW: the 25-75% width of the linear intensity profile across the tumor/lung boundary.

Figure 4.(A) Reconstructed thoracic images from both our adaptive and conventional protocols for trace ID m001 with respiratory and the two different amounts of cardiac motion. Insert highlights the region containing the spherical tumor. (B) Coronal view of the same volume. Insert highlights a section of the heart/lung boundary, red arrow indicates the region of largest motion. Intensity window display [-0.0387, 0.0303] mm⁻¹.

Figure 5. Boxplots of the ERW for all 17 traces using adaptive (blue) and the conventional (black) protocol in the AP direction with (A) 0.5 cm of cardiac motion and (B) 1.0 cm of cardiac motion and in the SI direction with (C) 0.5 cm of cardiac motion and (D) 1.0 cm of cardiac motion. For each box, the central line indicates the median, with the top and bottom edges indicating the 75th and 25th percentiles. The whiskers identify the maximum and minimum values of the data set.

This article is protected b

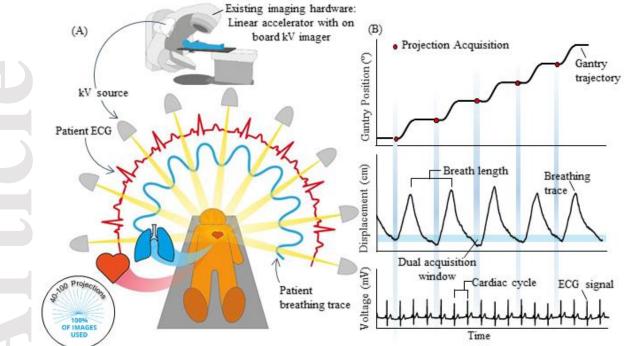
Figure 6. Boxplots of the CNR for all 17 traces using adaptive (blue) and the conventional (black) and protocol for (A) 0.5 cm of cardiac motion and (B) 1.0 cm of cardiac motion. For each box, the central line indicates the median, with the top and bottom edges indicating the 75th and 25th percentiles respectively. The whiskers identify the maximum and minimum values of the data set.

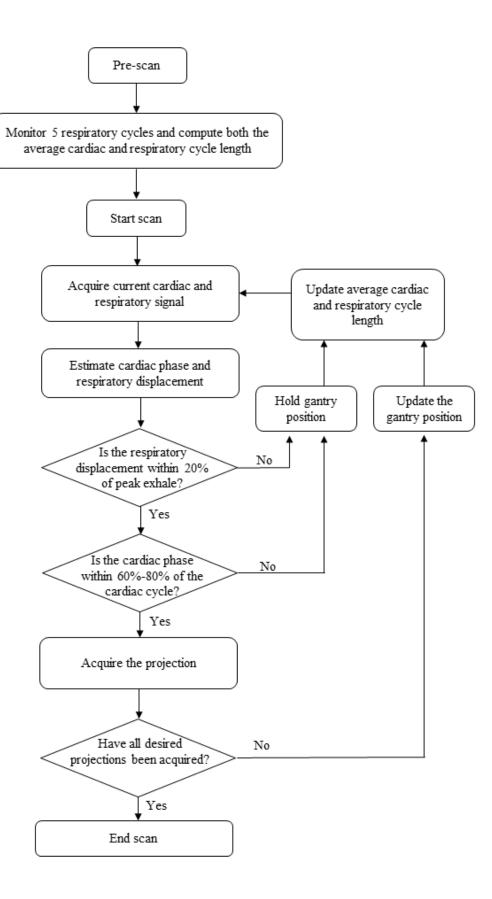
Trace ID	Heart Rate (bpm)	Breathing Rate (seconds) 3.0	
m001	67		
m002	63	3.3	
m003	68	3.4	
m004	64	2.9	
m005	71	3.4	
m007	56	4.5	
m008	101	2.6	
m009	64	5.7	
m010	59	3.2	
m011	70	3.0 2.5	
m012	68		
m013	74	3.7	
m014	65	4.0	
m015	63	3.2	
m016	80	3.9	
m017	76	3.3	
m019	66	2.6	

Table 1. Dual ECG and respiratory trace properties.

	Adaptive		Conventional	
Trace ID	40 Projections	75 Projections	100 Projections	1320 projections
m001	85 s	146 s	207 s	240 s
m002	161 s	286 s	376 s	240 s
m003	105 s	213 s	284 s	240 s
m004	128 s	242 s	320 s	240 s
m005	117 s	245 s	353 s	240 s
m007	173 s	318 s	435 s	240 s
m008	99 s	188 s	250 s	240 s
m009	144 s	258 s	337 s	240 s
m010	218 s	364 s	480 s	240 s
m011	111 s	218 s	291 s	240 s
m012	122 s	232 s	301 s	240 s
m013	115 s	230 s	320 s	240 s
m014	86 s	198 s	255 s	240 s
m015	128 s	217 s	296 s	240 s
m016	128 s	247 s	341 s	240 s
m017	121 s	212 s	278 s	240 s
m019	78 s	148 s	201 s	240 s

Table 2. Total scan times employing our adaptive and conventional protocols on a conventional linac.





This article is protected by copyright. All rights reserved.

